Clin Orthop Relat Res (2013) 471:1174–1185
DOI 10.1007/s11999-012-2487-0

Clinical Orthopaedics and Related Research®
A Publication of The Association of Bone and Joint Surgeons®

SYMPOSIUM: OSTEOCHONDRITIS DISSECANS

Oligo[poly(ethylene glycol)fumarate] Hydrogel Enhances Osteochondral Repair in Porcine Femoral Condyle Defects

James H. Hui FRCS, MD, Xiafei Ren PhD, Mohd Hassan Afizah MSc, Kerm Sin Chian PhD, Antonios G. Mikos PhD

Published online: 24 July 2012

Abstract

Background Management of osteochondritis dissecans remains a challenge. Use of oligo[poly(ethylene glycol)fumarate] (OPF) hydrogel scaffold alone has been reported in osteochondral defect repair in small animal models. However, preclinical evaluation of usage of this scaffold alone as a treatment strategy is limited.

Questions/purposes We therefore (1) determined in vitro pore size and mechanical stiffness of freeze-dried and rehydrated freeze-dried OPF hydrogels, respectively; (2) assessed in vivo gross defect filling percentage and histologic findings in defects implanted with rehydrated freeze-dried hydrogels for 2 and 4 months in a porcine model; (3) analyzed highly magnified histologic sections for different types of cartilage repair tissues, subchondral bone, and scaffold; and (4) assessed neotissue filling percentage, cartilage phenotype, and Wakitani scores.

Methods We measured pore size of freeze-dried OPF hydrogel scaffolds and mechanical stiffness of fresh and rehydrated forms. Twenty-four osteochondral defects from 12 eight-month-old micropigs were equally divided into scaffold and control (no scaffold) groups. Gross and histologic examination, one-way ANOVA, and one-way Mann-Whitney U test were performed at 2 and 4 months postoperatively.

Results Pore sizes ranged from 20 to 433 μm in diameter. Rehydrated freeze-dried scaffolds had mechanical stiffness of 1 MPa. The scaffold itself increased percentage of

One or more of the authors (JHH, XR), have received, during the study period, funding from Singapore National Medical Research Council (Grant Number NMRC 1142/2007).
All ICMJE Conflict of Interest Forms for authors and *Clinical Orthopaedics and Related Research* editors and board members are on file with the publication and can be viewed on request.
Clinical Orthopaedics and Related Research neither advocates nor endorses the use of any treatment, drug, or device. Readers are encouraged to always seek additional information, including FDA approval status, of any drug or device before clinical use.
Each author certifies that his or her institution approved the animal protocol for this investigation and that all investigations were conducted in conformity with ethical principles of research.
This work was performed at the Department of Orthopaedic Surgery, Yong Loo Lin School of Medicine, National University of Singapore, Singapore.

J. H. Hui (✉)
Cartilage Repair Program, Therapeutic Tissue Engineering Laboratory, Department of Orthopaedic Surgery, National University Health System, National University of Singapore, 1E, Kent Ridge Road, Singapore 119288, Singapore
e-mail: james_hui@nuhs.edu.sg; doshuij@nus.edu.sg

X. Ren
Department of Orthopaedic Surgery, Yong Loo Lin School of Medicine, National University of Singapore, Singapore, Singapore

M. H. Afizah
Department of Orthopaedic Surgery, National University Health System, National University Hospital, Singapore, Singapore

K. S. Chian
Division of Manufacturing, School of Mechanical and Aerospace Engineering, Nanyang Technological University, Singapore, Singapore

A. G. Mikos
Department of Chemical Engineering and Bioengineering, Rice University, Houston, TX, USA

neotissue filling at both 2 and 4 months to 58% and 54%, respectively, with hyaline cartilage making up 39% of neotissue at 4 months.

Conclusions Rehydrated freeze-dried OPF hydrogel can enhance formation of hyaline-fibrocartilaginous mixed repair tissue of osteochondral defects in a porcine model.

Clinical Relevance Rehydrated freeze-dried OPF hydrogel alone implanted into cartilage defects is insufficient to generate a homogeneously hyaline cartilage repair tissue, but its spacer effect can be enhanced by other tissue-regenerating mediators.

Introduction

Osteochondritis dissecans (OCD) is a focal lesion of the subchondral bone, characterized by the separation of an osteochondral fragment from the joint surface [2, 46]. Juvenile OCD lesions with an intact articular surface have a potential for healing through cessation of repetitive impact loading and have a higher potential of healing in children with open physis [2, 5, 33, 46]. However, surgery is considered with detached lesions in patients who do not have pain relief from nonoperative treatment [5, 16, 59].

Operative treatment of OCD includes transplantation of osteochondral autografts [9, 39, 64], microfracture [34, 51, 62], and autologous chondrocyte implantation [36, 47] combined with subchondral bone restoration [40, 52]. Osteochondral autograft offers the benefits of mature hyaline cartilage transplantation, primary bone healing, and quick recovery and is recommended for high-demand athletes but is limited by donor graft morbidity [10, 11]. Microfracture produces fibrocartilage and has inferior biomechanical properties [7, 15, 32, 38], while autologous chondrocyte implantation produces a better hybrid of fibrocartilage and hyaline cartilage [7, 32, 38, 51] but requires prolonged and complicated rehabilitation [34]. The use of scaffold alone offers a new strategy in the treatment of osteochondral injuries and diseases.

In a recent publication, both Guo et al. [13] and Kon et al. [35] found the implantation of scaffolds alone in defects of 3 and 7 mm in rabbit and sheep models, respectively, led to the formation of new chondral tissue that was hyaline, with zonal organization and intense staining for glycosaminoglycans (GAGs). The scaffold used in the investigation of Guo et al. [13] was oligo[poly(ethylene glycol)fumarate] (OPF) hydrogel. The OPF hydrogel is a well-studied scaffold [12, 13, 17–21, 26–30, 42–45, 49, 50, 54–58]. It possesses a higher water content than other hydrogels, such as poly(glycolic acid) and poly(L-lactic acid) polymer meshes. In addition, it is more biodegradable [19, 21, 26, 42, 54, 55, 58] and biocompatible [13, 17, 18, 57] compared to natural scaffold materials, such as gelatin, collagen, and hyaluronic acid [20]. In a preclinical evaluation of this scaffold, we investigated the effects of freeze-dried OPF hydrogel scaffold in a porcine model, which is more clinically relevant due to greater physiologic and anatomic similarities to humans. The freeze-dried scaffold will provide ease in transport, transfer, storage, and off-the-shelf commercialization.

We therefore (1) determined in vitro pore size and mechanical stiffness of freeze-dried and rehydrated freeze-dried OPF hydrogels, respectively; (2) assessed in vivo gross defect filling percentage and histologic findings in defects implanted with rehydrated freeze-dried hydrogels for 2 and 4 months in a porcine model; (3) analyzed highly magnified histologic sections for different types of cartilage repair tissues, subchondral bone, and scaffold; and (4) assessed neotissue filling percentage, cartilage phenotype, and Wakitani scores.

Materials and Methods

To investigate the effect that implantation of rehydrated freeze-dried OPF hydrogel has on cartilage repair of osteochondral defects in a porcine model (Fig. 1), we first synthesized the OPF hydrogel and characterized the gross structure (pore size) of freeze-dried hydrogel using scanning electron microscopy (SEM) and mechanical stiffness of fresh and rehydrated hydrogels using mechanical testing. We then created bicondylar defects in 12 skeletally mature PWG pigs, producing 24 defects. Twelve defects each were allocated to the scaffold and control (no scaffold) groups. Six pigs each were sacrificed at 2 and 4 months. Histologic sections from each sample were stained. We analyzed $\times 40$ and $\times 100$ magnification pictures for tissue filling and percentage of cartilage neotissue types through grid superimposition.

To determine the characteristics of the lyophilized OPF hydrogel, the scaffold was synthesized, lyophilized, and subsequently analyzed structurally and mechanically. Mechanical testing was performed to validate the rehydration process because the formation of ice crystals during the freeze-drying procedure could have damaged the scaffold's microstructure. Unless otherwise stated, all reagents used in this study were purchased from Sigma-Aldrich Co, LLC (St Louis, MO, USA). Antibodies were purchased from Chemicon (Temecula, CA, USA). OPF was synthesized by dissolving poly(ethylene glycol) (PEG) (MW 3450) in anhydrous methylene chloride. Fumaryl chloride and triethylamine were added dropwise into the PEG solution. The OPF was recrystallized twice and dried. The end group of OPF was characterized by nuclear magnetic resonance (NMR) after dissolving the OPF. The average molecular weight of OPF was calculated from the gel-permeation chromatography. The OPF was

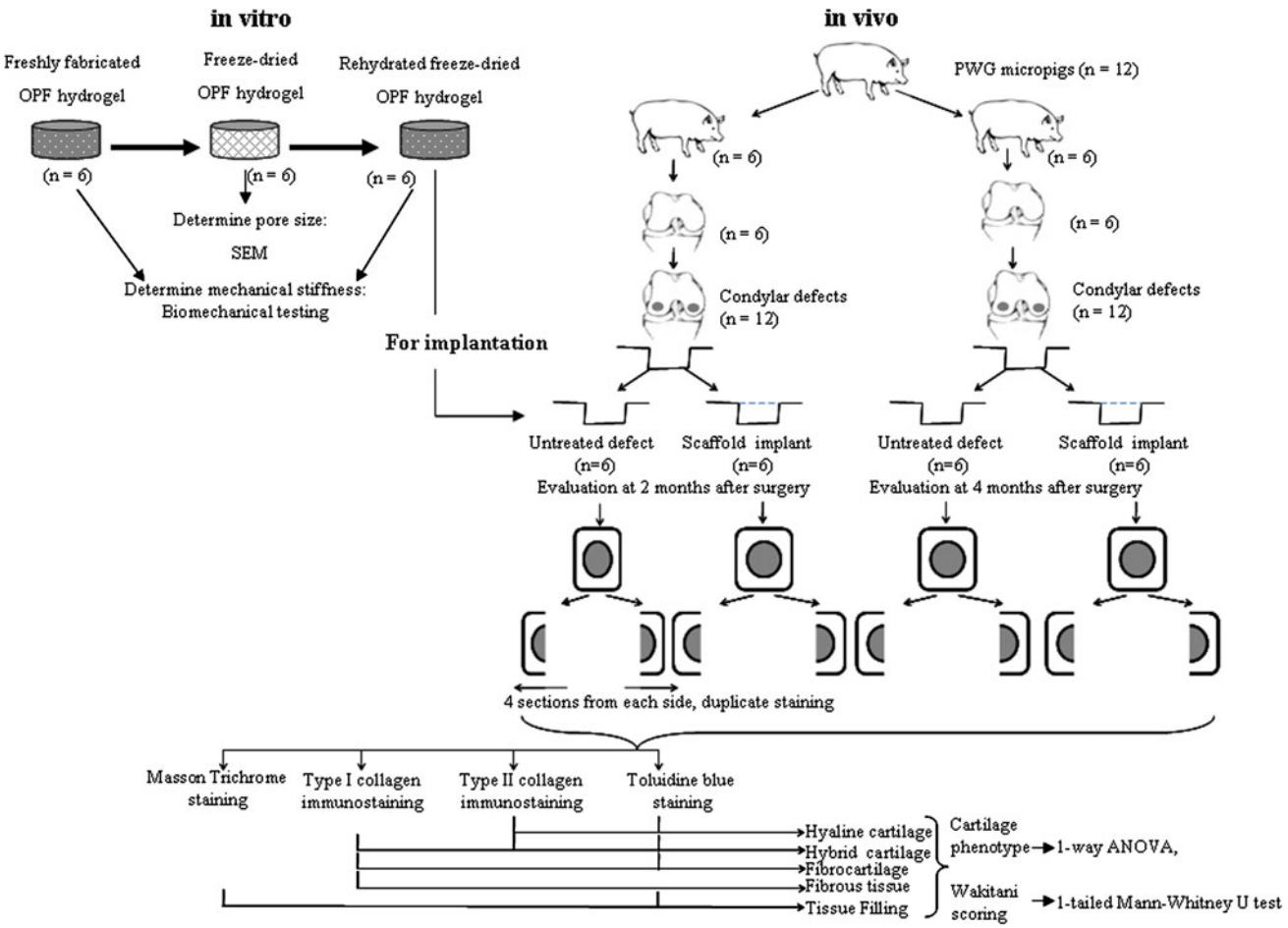

Fig. 1 A flow diagram shows the scope of the study, including sample number and statistical tests.

characterized using Fourier transform infrared and differential scanning calorimetry (Model 2920; TA Instruments, Newcastle, DE, USA) according to a published method [26]. The samples were analyzed at a heating rate of 10°C/minute from 0°C to 70°C. Fumarate hydrogel was fabricated with the OPF polymer and bisacrylamide according to a published method [17]. Briefly, OPF was dissolved in distilled water containing N,N′- methylene bisacrylamide as a crosslinking agent. Tetramethylethylenediamine and ammonium persulfate were added for crosslinking, after which gels were dialyzed, freeze-dried, and sliced into 1-mm-thick pieces. The scaffold was rehydrated with phosphate-buffered saline before filling of osteochondral defect.

To verify the pore sizes of the scaffold after the freeze-drying process, we performed SEM. Six samples were mounted onto specimen stubs, transferred to a vacuum desiccator for further water evaporation, and coated with a 50-nm gold layer using the sputter coater. SEM micrographs were obtained with a JEOL JSM5610LV microscope (JEOL Ltd, Tokyo, Japan) at 10 kV and ×50 magnification. Pore sizes were measured manually with a ruler; the average of the diameters of 100 pores each from six SEM micrographs was calculated.

To determine the hydrogel stiffness, six fresh hydrogel discs and six rehydrated freeze-dried hydrogels were examined with a microtester (EnduraTEC Systems Group, Bose Corp, Minnetonka, MN, USA). Samples were soaked in distilled water at room temperature and displacement was applied at 0.05 mm/second until 50% of sample depth. The stiffness modulus was calculated by the formula: modulus = stress/strain. The mean stiffness was calculated.

To investigate the in vivo ability of the rehydrated freeze-dried hydrogels to repair cartilage defects, we used 12 PWG micropigs (8 months old, skeletally mature, 20 kg, female) from PWG Genetics Pte Ltd (Singapore). All protocols had been approved by the Institutional Animal Care and Use Committee at our institution. The micropigs were anesthetized and a medial parapatellar incision and arthrotomy were then carried out at the right knee to expose the distal femur. Bicondylar osteochondral

defects (n = 24) (6-mm diameter, 1-mm depth) were created on the weightbearing region of the lateral and medial condyles (n = 12 each) with a 6-mm punch. The created chondral defects had a sharp edge, with a full layer of cartilage and a thin layer of subchondral bone removed (Fig. 2). An identical-sized rehydrated gel scaffold was press fit into one of the two defects (scaffold group) at random (opaque envelope method). The scaffold was kept in place by the close contact of the femoral condyle and meniscus. The other defect in the same knee was left empty for control. Wound closure was accomplished with bioabsorbable sutures. Animals were monitored until full recovery and allowed to move freely in cages, with adequate analgesia. Six animals each were euthanized with an overdose of barbiturates at 2 and 4 months postoperatively. After sacrifice, the defects on the lateral and medial condyles were photographed and processed for histologic analysis.

The extent of cartilage repair at the osteochondral defect was determined by histologic assessment. The 24 specimens from both the medial and lateral femoral condyles were fixed in 10% formalin, decalcified, and sectioned longitudinally from the middle part of the defect area into eight 5-μm-thick sections. Four stains were performed in duplicate: Masson trichrome (collagen), toluidine blue (GAG), and immunohistochemical staining for Types I and II collagen. Qualitative analysis of the neotissue was based on the cell morphology and extracellular matrix content. Hyaline cartilage is characterized by the presence of rounded cells in lacunae that express GAG and Type II collagen only. Fibrocartilage is defined by cells that produce GAG and Type I collagen only. Hybrid cartilage exhibits positive staining for both collagen types and GAG, while fibrous tissue is only positive for Type I collagen. We calculated the percentage of tissue filling in specimens using grid superimposition over the tissue slide. Three observers (XR, ZY, CTL; mean Fleiss' kappa = 0.72, 0.70, 0.65, respectively) evaluated the tissue filling percentage and neotissue phenotype and assessed the neotissue based on the scoring system of Wakitani et al. [60] to evaluate cell morphology, matrix staining, surface regularity, cartilage thickness, and integration with adjacent host cartilage (score of 0–14 points, with the best possible score being 0 and the worst 14) (Table 1).

Values are expressed as mean ± SD. We determined differences in repair cartilage phenotype and tissue filling percentages between the scaffold and control groups and between the 2- and 4-month time points using one-way ANOVA (VassarStats; http://vassarstats.net/anova1u.html). Wakitani scores of samples (n = 6) were compared using a one-way Mann-Whitney U test (http://elegans.som.vcu.edu/~leon/stats/utest.cgi).

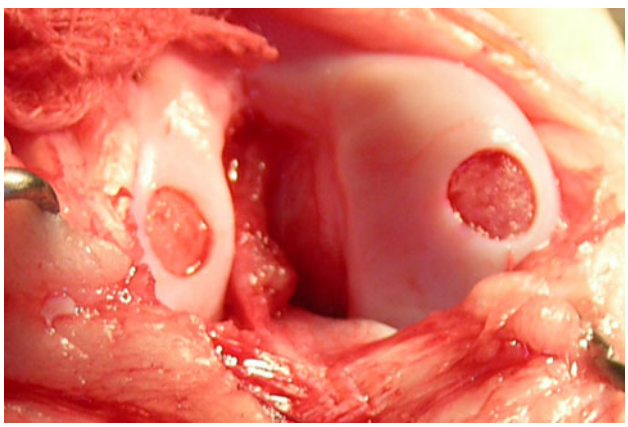

Fig. 2 A photograph shows the circular osteochondral defect immediately after creation, measuring 6 mm in diameter and 1 mm in depth.

Table 1. Histologic grading scale for the defects of cartilage [60]

Category	Points
Cell morphology	
Hyaline cartilage	0
Mostly hyaline cartilage	1
Mostly fibrocartilage	2
Mostly noncartilage	3
Noncartilage only	4
Matrix staining (metachromasia)	
Normal (compared with host adjacent cartilage)	0
Slightly reduced	1
Markedly reduced	2
No metachromatic stain	3
Surface regularity*	
Smooth (> 3/4)	0
Moderate (> 1/2–3/4)	1
Irregular (1/4–1/2)	2
Severely irregular (< 1/4)	3
Thickness of cartilage†	
> 2/3	0
1/3–2/3	1
< 1/3	2
Integration of donor with host adjacent cartilage	
Both edges integrated	0
One edge integrated	1
Neither edge integrated	2
Total maximum	14

* Total smooth area of the reparative cartilage compared with the entire area of the cartilage defect; †average thickness of the reparative cartilage compared with that of the surrounding cartilage. Reprinted with permission and © 1994 of The Journal of Bone and Joint Surgery, Inc, from Wakitani S, Goto T, Pineda SJ, Young RG, Mansour JM, Caplan AI, Goldberg VM. Mesenchymal cell-based repair of large, full-thickness defects of articular cartilage. *J Bone Joint Surg Am*. 1994;76:579–592.

Results

The lyophilization process turned the transparent OPF hydrogel (Fig. 3A) into a porous spongelike scaffold (Fig. 3B). SEM analysis revealed interconnected pores (Fig. 3C) 20 to 433 μm in diameter (136 ± 86 μm). Upon rehydration, water was first absorbed into the walls (Fig. 3D) before filling the remaining spaces. The mechanical stiffness of the rehydrated freeze-dried hydrogel was 0.97 MPa, which was slightly less than that of fresh hydrogel (1 MPa) (Fig. 4).

Gross morphologic (Fig. 5) and histologic (Fig. 6) observations revealed greater defect filling in the scaffold group compared to its control. The percentage filling (Table 2) was greater in the scaffold group (58%) at 2 months. By 4 months, the base of defects in the control group had been filled with cartilagelike tissue (Fig. 6C) and the percentage filling increased to 34%. The junction between the repaired tissue and subchondral bone was normal. In the scaffold group, the defect site and adjoined subchondral area were filled with regenerated tissue, which persisted at 54%. Degeneration of subchondral bone, noticeable through the loss of its native structure (Fig. 6A–B, 6D) was present in all groups except for the 4-month control group (Fig. 6C). In the scaffold group (Fig. 6B), undegraded scaffold could be seen at the topmost subchondral bone area.

Histologic observation of the 2-month control group revealed four distinct neotissue zones above the new subchondral bone contour line (Fig. 7). The upper defect area (Fig. 7A) contained fibrous tissue (Fig. 7C) while the lower central zone consisted of GAG (Fig. 7B)- and Type I collagen (Fig. 7B)-positive fibrocartilage. Hybrid cartilage consisting of GAG (Fig. 7B) and both collagen types (Fig. 7C–D) was noted at the junction between host subchondral bone and articular cartilage. In 2-month controls (Fig. 8A), hyaline cartilage, with columnar-organized cells positive for GAG (Fig. 8B) and Type II collagen (Fig. 8D) and negative for Type I collagen (Fig. 8C), could be located adjacent to the subchondral bone. This pattern was similarly observed in the 4-month control group and in the scaffold group at 2 months (Fig. 9) and 4 months. Quantitative data (Table 3) revealed a predominantly fibrous (72%) and fibrocartilaginous (62%) neotissue in the 2-month control and scaffold groups, respectively. At 4 months, the control group presented a homogeneous mix of hybrid, fibrous, and hyaline neocartilage, with fibrocartilage occupying the least volume, while the bulk of repair tissue in the scaffold group was hyaline. Scattered scaffold fragments in the trabecular bone area (Fig. 10) and numerous multinucleated osteoclasts alongside the scattered scaffold fragments (Fig. 11) were observed in the 2-month scaffold group. By 4 months, blood vessels were observed in the hollow areas of the scaffold group, which used to contain the OPF hydrogel fragments (Fig. 12).

The neotissue filling percentage of defects in the scaffold group at both time points was more than its control (Table 2). At 2 months, the level of fibrocartilage was higher while fibrous tissue was lower in the scaffold group (Table 3). At 4 months, the level of hyaline tissue was higher in the scaffold group. Across time points, there was a reduction in fibrocartilage tissue and an increase in both

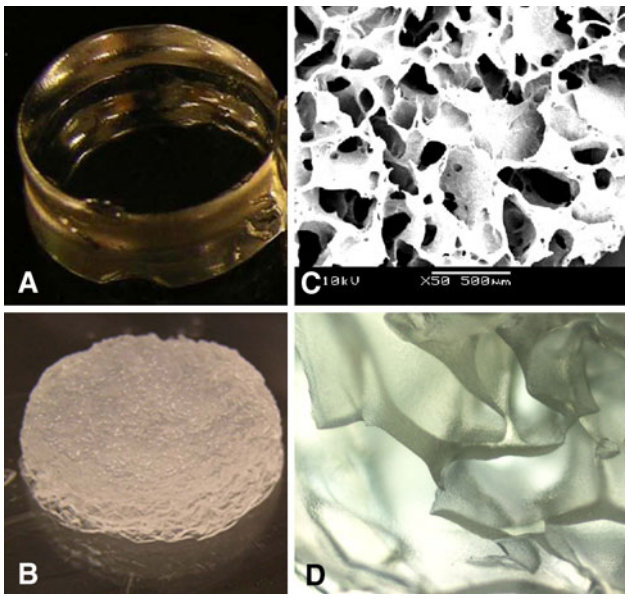

Fig. 3A–D The macromorphology of the OPF hydrogel is shown: (**A**) freshly synthesized hydrogel, (**B**) rehydrated freeze-dried hydrogel scaffold, (**C**) the porous structure of the freeze-dried hydrogel scaffold as observed under SEM (original magnification, ×50), and (**D**) a 50%-rehydrated freeze-dried hydrogel scaffold as seen under the phase-contrast microscope (original magnification, ×40).

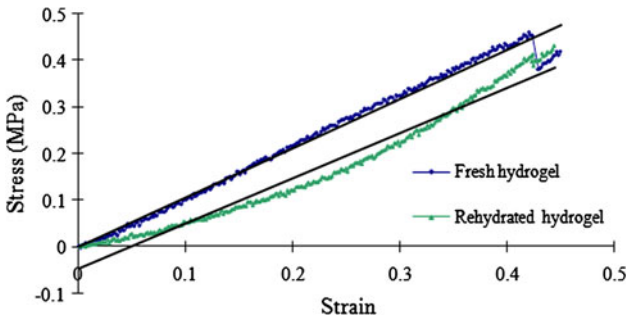

Fig. 4 The graph shows the relationship between strain and stress of the OPF scaffold in the freshly synthesized (blue) and rehydrated freeze-dried (green) states when subjected to compression of 0.05 mm/second until 50% of sample depth. The regression equations of the freshly synthesized and rehydrated hydrogels obtained from the graph are $y = 1.06x - 0.002$ ($R^2 = 0.985$) and $Y = 0.97x - 0.049$ ($R^2 = 0.966$), respectively. This leads to similar ($p = 0.185$) calculated mechanical stiffness values for freshly synthesized and rehydrated hydrogels of 1 (± 0.009) MPa and 0.97 (± 0.05) MPa, respectively.

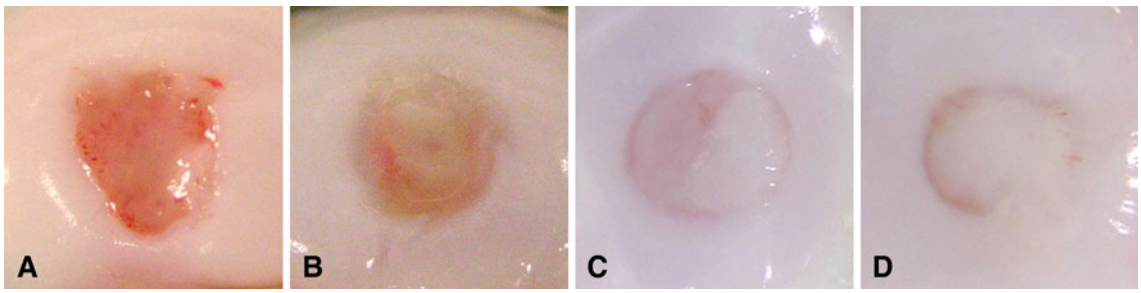

Fig. 5A–D Representative gross morphologic images of samples in the control and scaffold groups postoperatively are shown: (**A**) 2-month control group, (**B**) 2-month scaffold group, (**C**) 4-month control group, and (**D**) 4-month scaffold group.

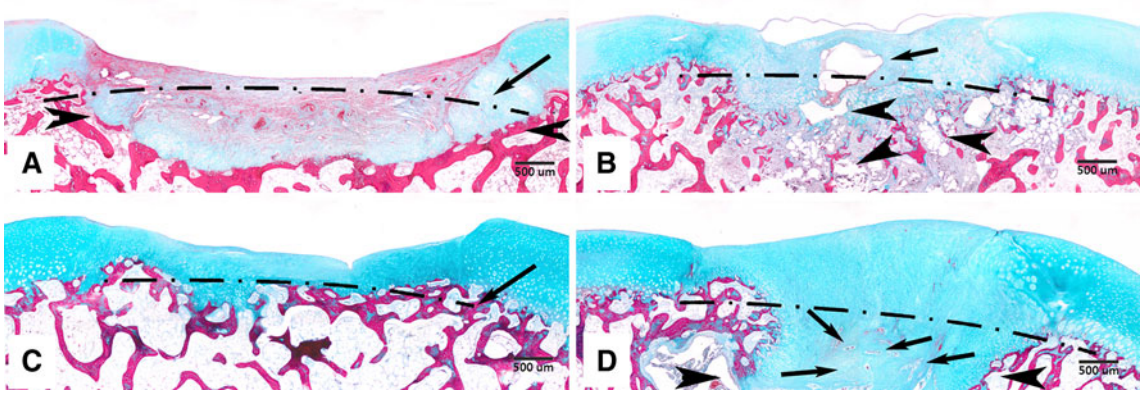

Fig. 6A–D Representative microscopic images of samples in the control and scaffold groups at 2 and 4 months postoperatively are shown (stain, Masson's trichrome; original magnification, ×40): (**A**) 2-month control group, (**B**) 2-month scaffold group, (**C**) 4-month control group, and (**D**) 4-month scaffold group. Dotted lines indicate the base of the created defects. (**A**) In the 2-month control group, degeneration of subchondral bone is observed through the loss of its native structure (arrowheads). (**B**) In the 2-month scaffold group, undegraded scaffold can be seen in the neotissue (arrow) and in subchondral bone (arrowheads). (**C**) In the 4-month control group, the base of the defect has been filled with a thin layer of cartilagelike tissue and the subchondral bone structure is observed to resemble its native state. (**D**) In the 4-month scaffold group, the repair tissue is observed to fill the majority of the defect space. The area previously occupied by degenerated subchondral bone has been replaced with cartilagelike tissue (between the two arrowheads), including the presence of tiny scaffold fragments (arrows).

Table 2. Neotissue percentage in defects

Variable	Two months		Four months	
	Control group	Scaffold group	Control group	Scaffold group
Neoformed tissue filling ratio*	29.3 ± 14.1	58.0 ± 15.1	34.2 ± 10.5	54.1 ± 11.3
p value				
Two-month control group		0.007	0.513	0.006
Two-month scaffold group	0.007		0.010	0.621
Four-month control group	0.513	0.010		0.008
Four-month scaffold group	0.006	0.621	0.008	

* Neoformed tissue filling ratio is a percentage of the total tissue against the area of the defect (expressed as mean ± SD); the tissue below the original contour line of the subchondral bone is not included; differences were determined by one-way ANOVA.

hyaline cartilage and hybrid cartilage in the scaffold group. The Wakitani scores (Table 4) of the neotissue in defects of the scaffold group at both time points were lower than their respective controls, but only the neotissue arising from scaffold treatment at 2 months attained better scores than its control.

Discussion

Symptomatic OCD of the knee is a challenging clinical problem [16, 46, 59]. Tissue-engineering approaches to repair osteochondral defects have therefore attracted increasing attention. Guo et al. [13] reported the

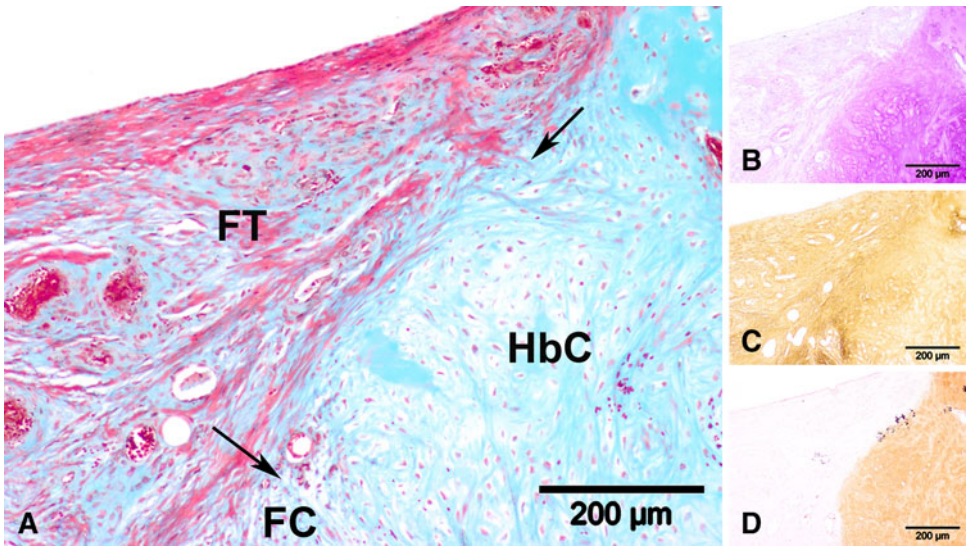

Fig. 7A–D Representative high-magnification microscopic images taken from the central section of the slide (original magnification, ×100) of a sample from the control group at 2 months postoperatively are shown: (**A**) Masson's trichrome staining, (**B**) toluidine blue staining, (**C**) Type I collagen immunostaining, and (**D**) Type II collagen immunostaining. Neotissue in this view consists of fibrous tissue (FT), fibrocartilage (FC), and hybrid cartilage (HbC). The arrows indicate the boundary between the different tissue types. The fibrous tissue is (**B**) GAG-negative, (**C**) Type I collagen-positive, and (**D**) Type II collagen-negative. The fibrocartilage is (**B**) GAG-positive, (**C**) Type I collagen-positive, and (**D**) Type II collagen-negative. (**B–D**) The hybrid cartilage is positive for all three stainings.

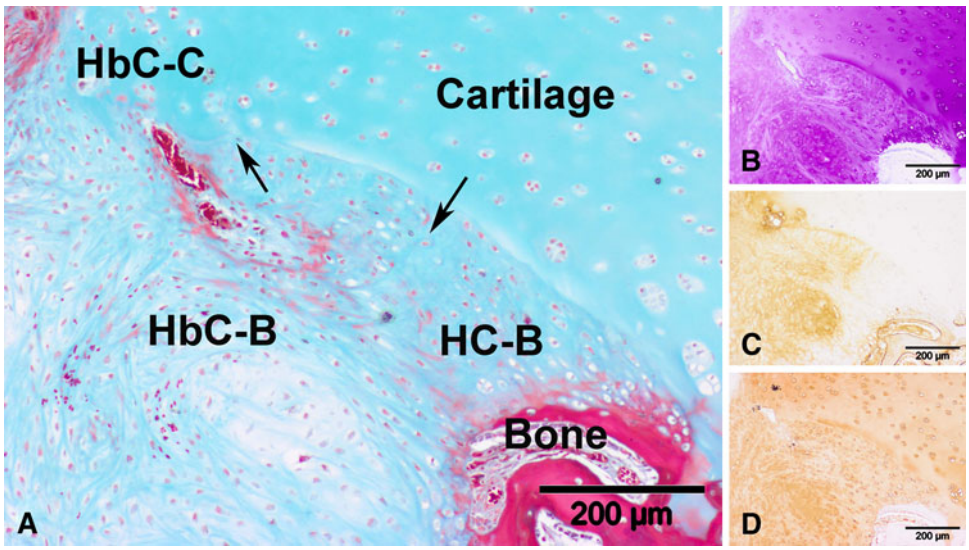

Fig. 8A–D Representative high-magnification microscopic images taken from the right lowermost section of the slide (original magnification, ×100) of a sample from the control group at 2 months postoperatively are shown: (**A**) Masson's trichrome staining, (**B**) toluidine blue staining, (**C**) Type I collagen immunostaining, and (**D**) Type II collagen immunostaining. Neotissue in this view consists of hyaline cartilage (HC) and hybrid cartilage (HbC) of which we postulate the source to be bone (-B) and cartilage (-C). The arrows indicate the boundary between the different tissue types. The hyaline cartilage is (**B**) GAG-positive, (**C**) Type I collagen-negative, and (**D**) Type II collagen-positive. (**B–D**) The hybrid cartilage is positive for all three stainings.

implantation of OPF hydrogels alone in osteochondral defects led to the formation of hyaline cartilage. OPF hydrogel is a polymer created through the synthesis of fumaric acid and PEG through ester bonds [26]. The ability of the ester bonds to undergo hydrolysis under acidic and basic conditions confers biodegradable characteristics, of which in vitro [19, 21, 26, 42, 54, 55, 58] and in vivo [13, 17, 18, 57] degradation rates have been reported. It is also biocompatible, evident from in vitro [12, 42–44, 50, 55, 56, 58] and in vivo [13, 17, 18, 57] assessments. These characteristics have led to numerous in vitro [12, 20, 21, 27–30, 43–45, 56] and rabbit model studies [13, 17, 18, 57]. A preclinical evaluation of the usage of this scaffold alone as a treatment strategy is lacking. We therefore

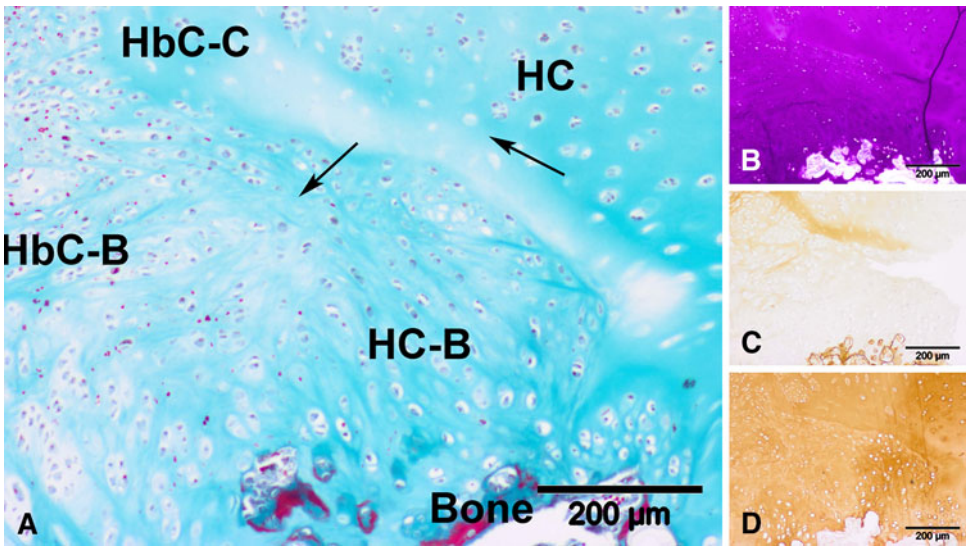

Fig. 9A–D Representative high-magnification microscopic images taken from the right lowermost section of the slide (original magnification, ×100) of a sample from the scaffold group at 2 months postoperatively are shown: (**A**) Masson's trichrome staining, (**B**) toluidine blue staining (**C**) Type I collagen immunostaining, and (**D**) Type II collagen immunostaining. Neotissue in this view consists of hyaline cartilage (HC) and hybrid cartilage (HbC) of which we postulate the source to be bone (-B) and cartilage (-C). The arrows indicate the boundary between the different tissue types. The hyaline cartilage is (**B**) GAG-positive, (**C**) Type I collagen-negative, and (**D**) Type II collagen-positive. (**B–D**) The hybrid cartilage is positive for all three stainings.

Table 3. Analysis of neotissue phenotypes

Score parameter	Content (%)*				p value			
	Two months		Four months					
	Control group	Scaffold group	Control group	Scaffold group	Two-month control group versus 2-month scaffold group	Four-month control group versus 4-month scaffold group	Two-month control group versus 4-month control group	Two-month scaffold group versus 4-month scaffold group
Hyaline cartilage	2.5 ± 3.2	6.4 ± 8.8	21.5 ± 14.6	38.9 ± 8.0	0.334	0.029	0.011	< 0.0001
Hybrid cartilage	19.0 ± 5.6	7.8 ± 5.0	22.0 ± 9.3	29.3 ± 13.5	0.004	0.301	0.513	0.004
Fibrocartilage	6.2 ± 5.4	62.2 ± 26.1	12.0 ± 3.4	9.5 ± 4.8	0.0004	0.334	0.049	0.0007
Fibrous tissue	72.3 ± 11.5	9.9 ± 16.8	21.9 ± 14.7	9.8 ± 9.0	< 0.0001	0.116	0.217	1.000

* Content of the hyaline, fibrocartilage, hybrid cartilage, and fibrous tissue is a percentage of the total tissue located at the defect area (expressed as mean ± SD); the tissue below the original contour line of the subchondral bone was not included; differences were determined by one-way ANOVA.

(1) determined in vitro pore size and mechanical stiffness of freeze-dried and rehydrated freeze-dried OPF hydrogels, respectively; (2) assessed in vivo gross defect filling percentage and histologic findings in defects implanted with rehydrated freeze-dried hydrogels for 2 and 4 months in a porcine model; (3) analyzed highly magnified histologic sections for different types of cartilage repair tissues, subchondral bone, and scaffold; and (4) assessed neotissue filling percentage, cartilage phenotype, and Wakitani scores.

We acknowledge the limitations of our study. First, high porcine maintenance costs limited our study to 12 micropigs. However, to increase the number of samples (if not independent), we created bicondylar defects to double the sample size. Second, although complete hyaline repair was not achieved, we are not surprised as this is a short-term study and increased maturation into hyaline tissue was observed. It is possible complete repair can be obtained with longer postoperative periods and this will be investigated in future studies. Third, the pathophysiologic environment of the defect in this study would at best only replicate an acute osteochondral injury. Fourth, a quicker restoration to normal state may be possible if anisotropic OPF hydrogel scaffolds are developed in the future as

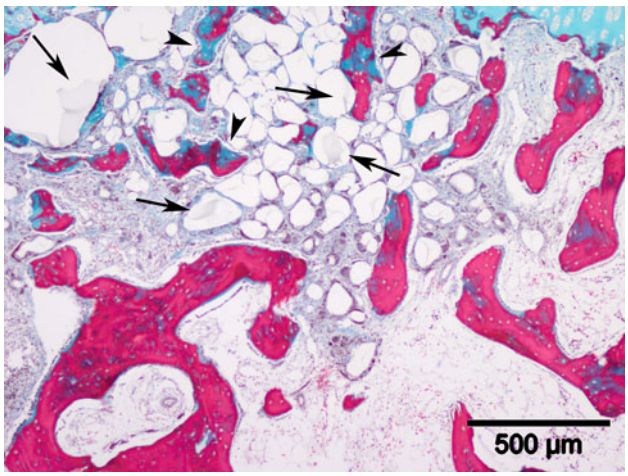

Fig. 10 A microscopic image illustrates broken scaffold fragments (arrows) scattered in the trabecular bone area in the defect of a 2-month scaffold group sample (stain, Masson's trichrome; original magnification, ×40). The trabecular bones (arrowheads) near these scaffolds are thinner and smaller and are not homogeneously stained.

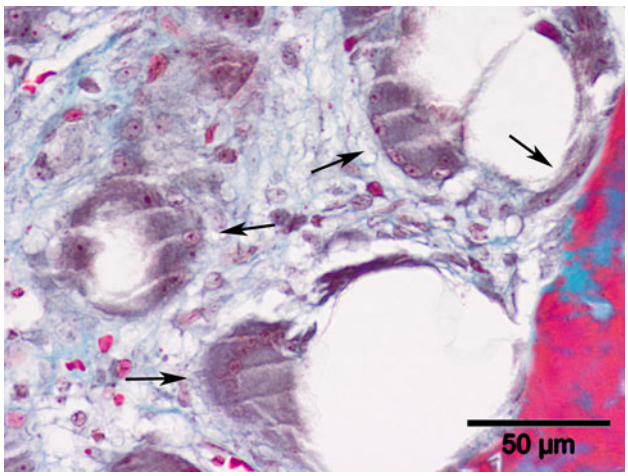

Fig. 11 This highly magnified microscopic image of a sample from a 2-month scaffold group sample (stain, Masson's trichrome; original magnification, ×400) shows large multinucleated cells (arrows) among the scaffold fragments surrounding the trabecular bone area.

currently the development of anisotropic tissue only occurs after scaffold degradation.

We explored rehydrated freeze-dried OPF hydrogel as a scaffold due to its ready-to-use form. The process of freeze-drying did not cause any shrinkage in physical structure or affect the scaffold's mechanical stiffness, as seen in the slight reduction in its mechanical stiffness when compared against that of fresh OPF hydrogel. An added advantage of freeze-drying is the creation of pores, as reported by Kato and Gehrke [31]. The pore sizes would be expected to be reduced on rehydration. Nonetheless, the presence of pores could be beneficial since scaffold pore sizes reportedly affect cellular proliferation [23] and

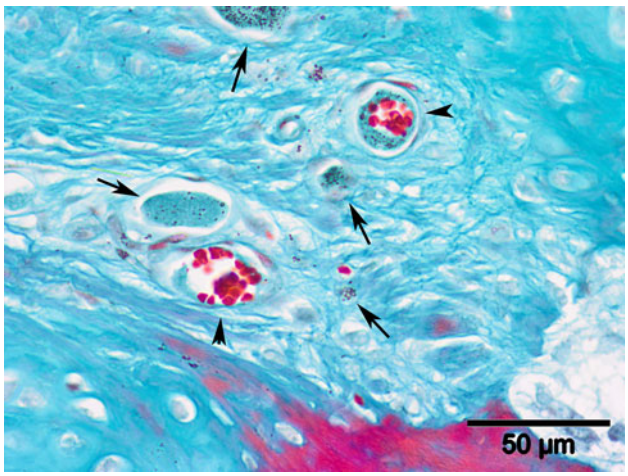

Fig. 12 A close-up view of scattered scaffold fragments (arrows) in the degenerated subchondral bone of a 4-month scaffold group sample is shown (stain, Masson's trichrome; original magnification, ×400). The scaffold fragments are stained and blood vessels can be clearly seen (arrowheads) in the middle of the hollow spaces, which were previously occupied by the degraded scaffold fragments.

differentiation [53], which play important roles in repair tissue regeneration.

Defects in the scaffold group at both time points were 57% to 54% filled by repair tissue, while less filling was achieved in the control. This is contrary to OPF hydrogel implantation in a rabbit model, where the osteochondral defect was fully packed with repair tissue at 3 months postoperatively [13]. More than 90% tissue filling was also noted in 2.4-mm [63] and 3.7-mm [41] defects of the rabbit model, which were left untreated for 2 and 3 months, respectively. However, osteochondral defects implanted with hydrogel scaffolds generally have incomplete filling in large animals [14, 48]. Differences in repair could be attributed to different intrinsic spontaneous healing capacities between species, as shown by Kon et al. who reported the implantation of the same collagen-hydroxyapatite scaffold into sheep [35] and equine [37] models generated inferior fibrocartilaginous tissue in the larger-sized animal. Despite the worse repair in our porcine model compared to the rabbit model [13], our results are clinically more relevant due to closer anatomic similarities of the porcine model to humans.

Cartilage maturation was observed in the scaffold group, evident from increased amounts of hyaline cartilage as time progressed from 2 to 4 months. The quality of repair cartilage again did not resemble the native cartilage structure obtained in the rabbit model [13] and could be due to different spontaneous healing abilities, as pointed out earlier. Another possible explanation would be that a longer postoperative time is required for repair tissue remodeling. This is supported by studies carried out in sheep [14] and canine [61] models, where emergence of repair tissue

Table 4. Histologic scores of neotissue at 2 and 4 months

Score parameter	Histologic score (points)*				p value			
	Two months		Four months					
	Control group	Scaffold group	Control group	Scaffold group	Two-month control group versus 2-month scaffold group	Four-month control group versus 4-month scaffold group	Two-month control group versus 4-month control group	Two-month scaffold group versus 4-month scaffold group
Tissue morphology	2.5 ± 0.5	1.8 ± 0.4	1.8 ± 0.4	1.7 ± 0.5	0.046	0.315	0.046	0.350
Matrix staining	1.8 ± 0.4	1.5 ± 0.5	0.3 ± 0.5	0.5 ± 0.8	0.168	0.436	0.003	0.027
Surface regularity	2.8 ± 0.4	2.0 ± 0.6	2.3 ± 0.5	1.5 ± 1.2	0.023	0.131	0.075	0.288
Thickness of cartilage	1.5 ± 0.5	1.2 ± 0.8	1.7 ± 0.8	1.2 ± 0.8	0.236	0.189	0.405	0.500
Integration with host	0 ± 0	0 ± 0	0 ± 0	0 ± 0	0.500	0.500	0.500	0.500
Total	8.7 ± 1.5	6.5 ± 0.5	6.2 ± 2.3	4.8 ± 3.3	0.013	0.168	0.010	0.115

* Histologic score (expressed as mean ± SD) is based on the grading scale of Wakatani et al. [60] (total score = 0–14; best possible score = 0, worst possible score = 14; for a description of the grading scale, see Table 1); differences were determined by one-way Mann-Whitney U tests.

resembling native cartilage structure occurred after 6 months. It was surprising to find the quality of repair tissue in our control group surpassed the thin layer of sparsely populated fibrous tissue, commonly found to occupy the osteochondral defects of large-animal models [14, 25]. This was despite the use of skeletally mature animals, as germinal cells from the physis of skeletally immature animals [1] could contribute to cartilage regeneration. The creation of a large-sized 6-mm defect was decided on to mimic the acute damage experienced in OCD and also to minimize effects of spontaneous healing, as supported by the findings of Jackson et al. [24] that 6-mm osteochondral defects in the goat model did not heal spontaneously.

High-magnification images of serial histologic sections in both control and scaffold groups revealed the possible cellular origin of the repair tissue, deducible from the close proximity and morphologic resemblance to the cells located in direct contact, and spanning the distance between the neotissue and host cartilage and bone. It led us to postulate the origins of repair tissues in this study were mostly bone and cartilage. We cannot confidently conclude there were no other sources as Hunziker and Rosenberg [22] also published a similar finding based on histologic proof, where the synovial membrane was concluded to have contributed to tissue repair.

Complete integration was noted between neotissue and host cartilage and subchondral bone, similar to osteochondral repair reported in other publications [41, 61]. However, despite the cartilage healing observed, regeneration of trabecular subchondral bone did not occur even at 4 months. Instead, subchondral resorption took place; this was unique to the scaffold group and was also not observed in the rabbit model [13]. It is probable scaffold degradation in the porcine model weakened the trabecular bone, which triggered the eventual subchondral resorption by the detected osteoclasts. The rate of scaffold degradation in the porcine model was comparable to that in the rabbit model, where complete scaffold degradation in a fraction of samples occurred within 3 months [13]. The co-appearance of blood vessels in the hollow spaces occupied with scaffold fragments could indicate the scaffold fragments were removed through vascularization.

The presence of a greater proportion of hyaline cartilage tissue in scaffold group defects at both time points indicated the OPF hydrogel scaffold enhanced the formation of predominantly hyaline cartilage tissue. This is promising as other osteochondral defect treatments with scaffold only [4, 8, 14] result in the predominant formation of fibrocartilage, which possesses inferior biomechanical properties [6] and would translate to a shorter repair tissue life span [3].

OPF hydrogel scaffold enhanced cartilage regeneration, without inducing subchondral regeneration. Usage of rehydrated freeze-dried OPF hydrogel alone is insufficient to generate a homogeneously hyaline cartilage repair tissue, but its spacer effect can be enhanced by other tissue-regenerating mediators.

Acknowledgments We thank Chin Tat Lim, MBBS, Zheng Yang, PhD, Yingnan Wu, MSc, and Awang Shukrimi, MBBS, for help with animal surgery, SEM, mechanical testing, histologic analysis, and write-up of the initial draft.

References

1. Chu CR, Szczodry M, Bruno S. Animal models for cartilage regeneration and repair. *Tissue Eng Part B Rev.* 2010;16:105–115.
2. Crawford DC, Safran MR. Osteochondritis dissecans of the knee. *J Am Acad Orthop Surg.* 2006;14:90–100.
3. Ferkel RD, Zanotti RM, Komenda GA, Sgaglione NA, Cheng MS, Applegate GR, Dopirak RM. Arthroscopic treatment of

chronic osteochondral lesions of the talus: long-term results. *Am J Sports Med*. 2008;36:1750–1762.
4. Filová E, Rampichová M, Handl M, Lytvynets A, Halouzka R, Usvald D, Hlucilová J, Procházka R, Dezortová M, Rolencová E, Kostáková E, Trc T, Stastný E, Kolácná L, Hájek M, Motlík J, Amler E. Composite hyaluronate-type I collagen-fibrin scaffold in the therapy of osteochondral defects in miniature pigs. *Physiol Res.* 2007;56(suppl 1):S5–S16.
5. Flynn JM, Kocher MS, Ganley TJ. Osteochondritis dissecans of the knee. *J Pediatr Orthop.* 2004;24:434–443.
6. Freemont AJ, Hoyland J. Lineage plasticity and cell biology of fibrocartilage and hyaline cartilage: its significance in cartilage repair and replacement. *Eur J Radiol.* 2006;57:32–36.
7. Gobbi A, Nunag P, Malinowski K. Treatment of full thickness chondral lesions of the knee with microfracture in a group of athletes. *Knee Surg Sports Traumatol Arthrosc.* 2005;13:213–221.
8. Gotterbarm T, Richter W, Jung M, Berardi Vilei S, Mainil-Varlet P, Yamashita T, Breusch SJ. An in vivo study of a growth-factor enhanced, cell free, two-layered collagen-tricalcium phosphate in deep osteochondral defects. *Biomaterials.* 2006;27:3387–3395.
9. Gudas R, Kalesinskas RJ, Kimtys V, Stankevicius E, Toliusis V, Bernotavicius G, Smailys A. A prospective randomized clinical study of mosaic osteochondral autologous transplantation versus microfracture for the treatment of osteochondral defects in the knee joint in young athletes. *Arthroscopy.* 2005;21:1066–1075.
10. Guettler JH, Demetropoulos CK, Yang KH, Jurist KA. Osteochondral defects in the human knee: influence of defect size on cartilage rim stress and load redistribution to surrounding cartilage. *Am J Sports Med.* 2004;32:1451–1458.
11. Guettler JH, Demetropoulos CK, Yang KH, Jurist KA. Dynamic evaluation of contact pressure and the effects of graft harvest with subsequent lateral release at osteochondral donor sites in the knee. *Arthroscopy.* 2005;21:715–720.
12. Guo X, Park H, Liu G, Liu W, Cao Y, Tabata Y, Kasper FK, Mikos AG. In vitro generation of an osteochondral construct using injectable hydrogel composites encapsulating rabbit marrow mesenchymal stem cells. *Biomaterials.* 2009;30:2741–2752.
13. Guo X, Park H, Young S, Kretlow JD, van den Beucken JJ, Baggett LS, Tabata Y, Kasper FK, Mikos AG, Jansen JA. Repair of osteochondral defects with biodegradable hydrogel composites encapsulating marrow mesenchymal stem cells in a rabbit model. *Acta Biomater.* 2010;6:39–47.
14. Hao T, Wen N, Cao JK, Wang HB, Lü SH, Liu T, Lin QX, Duan CM, Wang CY. The support of matrix accumulation and the promotion of sheep articular cartilage defects repair in vivo by chitosan hydrogels. *Osteoarthritis Cartilage.* 2010;18:257–265.
15. Harris JD, Siston RA, Brophy RH, Lattermann C, Carey JL, Flanigan DC. Failures, re-operations, and complications after autologous chondrocyte implantation—a systematic review. *Osteoarthritis Cartilage.* 2011;19:779–791.
16. Hayan R, Phillipe G, Ludovic S, Claude K, Jean-Michel C. Juvenile osteochondritis of femoral condyles: treatment with transchondral drilling: analysis of 40 cases. *J Child Orthop.* 2010;4:39–44.
17. Holland TA, Bodde EW, Baggett LS, Tabata Y, Mikos AG, Jansen JA. Osteochondral repair in the rabbit model utilizing bilayered, degradable oligo(poly(ethylene glycol) fumarate) hydrogel scaffolds. *J Biomed Mater Res A.* 2005;75:156–167.
18. Holland TA, Bodde EW, Cuijpers VM, Baggett LS, Tabata Y, Mikos AG, Jansen JA. Degradable hydrogel scaffolds for in vivo delivery of single and dual growth factors in cartilage repair. *Osteoarthritis Cartilage.* 2007;15:187–197.
19. Holland TA, Tabata Y, Mikos AG. In vitro release of transforming growth factor-beta 1 from gelatin microparticles encapsulated in biodegradable, injectable oligo(poly(ethylene glycol) fumarate) hydrogels. *J Control Release.* 2003;91:299–313.
20. Holland TA, Tabata Y, Mikos AG. Dual growth factor delivery from degradable oligo(poly(ethylene glycol) fumarate) hydrogel scaffolds for cartilage tissue engineering. *J Control Release.* 2005;101:111–125.
21. Holland TA, Tessmar JK, Tabata Y, Mikos AG. Transforming growth factor-beta 1 release from oligo(poly(ethylene glycol) fumarate) hydrogels in conditions that model the cartilage wound healing environment. *J Control Release.* 2004;94:101–114.
22. Hunziker EB, Rosenberg LC. Repair of partial-thickness defects in articular cartilage: cell recruitment from the synovial membrane. *J Bone Joint Surg Am.* 1996;78:721–733.
23. Hwang CM, Sant S, Masaeli M, Kachouie NN, Zamanian B, Lee SH, Khademhosseini A. Fabrication of three-dimensional porous cell-laden hydrogel for tissue engineering. *Biofabrication.* 2010;2:035003.
24. Jackson DW, Lalor PA, Aberman HM, Simon TM. Spontaneous repair of full-thickness defects of articular cartilage in a goat model: a preliminary study. *J Bone Joint Surg Am.* 2001;83:53–64.
25. Jiang CC, Chiang H, Liao CJ, Lin YJ, Kuo TF, Shieh CS, Huang YY, Tuan RS. Repair of porcine articular cartilage defect with a biphasic osteochondral composite. *J Orthop Res*. 2007;25:1277–1290.
26. Jo S, Shin H, Shung AK, Fisher JP, Mikos AG. Synthesis and characterization of oligo(poly(ethylene glycol) fumarate) macromer. *Macromolecules* 2001;34:2839–2844.
27. Kasper FK, Jerkins E, Tanahashi K, Barry MA, Tabata Y, Mikos AG. Characterization of DNA release from composites of oligo(poly(ethylene glycol) fumarate) and cationized gelatin microspheres in vitro. *J Biomed Mater Res A*. 2006;78:823–835.
28. Kasper FK, Kushibiki T, Kimura Y, Mikos AG, Tabata Y. In vivo release of plasmid DNA from composites of oligo(poly(ethylene glycol)fumarate) and cationized gelatin microspheres. *J Control Release.* 2005;107:547–561.
29. Kasper FK, Seidlits SK, Tang A, Crowther RS, Carney DH, Barry MA, Mikos AG. In vitro release of plasmid DNA from oligo(poly(ethylene glycol) fumarate) hydrogels. *J Control Release.* 2005;104:521–539.
30. Kasper FK, Young S, Tanahashi K, Barry MA, Tabata Y, Jansen JA, Mikos AG. Evaluation of bone regeneration by DNA release from composites of oligo(poly(ethylene glycol) fumarate) and cationized gelatin microspheres in a critical-sized calvarial defect. *J Biomed Mater Res A.* 2006;78:335–342.
31. Kato N, Gehrke SH. Microporous, fast response cellulose ether hydrogel prepared by freeze-drying. *Colloids Surf B Biointerfaces*. 2004;38:191–196.
32. Knutsen G, Engebretsen L, Ludvigsen TC, Drogset JO, Grøntvedt T, Solheim E, Strand T, Roberts S, Isaksen V, Johansen O. Autologous chondrocyte implantation compared with microfracture in the knee: a randomized trial. *J Bone Joint Surg Am.* 2004;86:455–464.
33. Kocher MS, Tucker R, Ganley TJ, Flynn JM. Management of osteochondritis dissecans of the knee: current concepts review. *Am J Sports Med*. 2006;34:1181–1191.
34. Kon E, Filardo G, Berruto M, Benazzo F, Zanon G, Della Villa S, Marcacci M. Articular cartilage treatment in high-level male soccer players: a prospective comparative study of arthroscopic second-generation autologous chondrocyte implantation versus microfracture. *Am J Sports Med.* 2011;39:2549–2557.
35. Kon E, Filardo G, Delcogliano M, Fini M, Salamanna F, Giavaresi G, Martin I, Marcacci M. Platelet autologous growth factors decrease the osteochondral regeneration capability of a collagen-hydroxyapatite scaffold in a sheep model. *BMC Musculoskelet Disord.* 2010;11:220.

36. Kon E, Gobbi A, Filardo G, Delcogliano M, Zaffagnini S, Marcacci M. Arthroscopic second-generation autologous chondrocyte implantation compared with microfracture for chondral lesions of the knee: prospective nonrandomized study at 5 years. *Am J Sports Med.* 2009;37:33–41.
37. Kon E, Mutini A, Arcangeli E, Delcogliano M, Filardo G, Nicoli Aldini N, Pressato D, Quarto R, Zaffagnini S, Marcacci M. Novel nanostructured scaffold for osteochondral regeneration: pilot study in horses. *J Tissue Eng Regen Med.* 2010;4:300–308.
38. Kreuz PC, Erggelet C, Steinwachs MR, Krause SJ, Lahm A, Niemeyer P, Ghanem N, Uhl M, Südkamp N. Is microfracture of chondral defects in the knee associated with different results in patients aged 40 years or younger? *Arthroscopy.* 2006;22: 1180–1186.
39. Miura K, Ishibashi Y, Tsuda E, Sato H, Toh S. Results of arthroscopic fixation of osteochondritis dissecans lesion of the knee with cylindrical autogenous osteochondral plugs. *Am J Sports Med.* 2007;35:216–222.
40. Ochs BG, Müller-Horvat C, Albrecht D, Schewe B, Weise K, Aicher WK, Rolauffs B. Remodeling of articular cartilage and subchondral bone after bone grafting and matrix-associated autologous chondrocyte implantation for osteochondritis dissecans of the knee. Am *J Sports Med.* 2011;39:764–773.
41. Oshima Y, Harwood FL, Coutts RD, Kubo T, Amiel D. Variation of mesenchymal cells in polylactic acid scaffold in an osteochondral repair model. *Tissue Eng Part C Methods*. 2009;15:595–604.
42. Park H, Guo X, Temenoff JS, Tabata Y, Caplan AI, Kasper FK, Mikos AG. Effect of swelling ratio of injectable hydrogel composites on chondrogenic differentiation of encapsulated rabbit marrow mesenchymal stem cells in vitro. *Biomacromolecules.* 2009;10:541–546.
43. Park H, Temenoff JS, Holland TA, Tabata Y, Mikos AG. Delivery of TGF-beta1 and chondrocytes via injectable, biodegradable hydrogels for cartilage tissue engineering applications. *Biomaterials.* 2005;26:7095–7103.
44. Park H, Temenoff JS, Tabata Y, Caplan AI, Mikos AG. Injectable biodegradable hydrogel composites for rabbit marrow mesenchymal stem cell and growth factor delivery for cartilage tissue engineering. *Biomaterials.* 2007;28:3217–3227.
45. Park H, Temenoff JS, Tabata Y, Caplan AI, Raphael RM, Jansen JA, Mikos AG. Effect of dual growth factor delivery on chondrogenic differentiation of rabbit marrow mesenchymal stem cells encapsulated in injectable hydrogel composites. *J Biomed Mater Res A.* 2009;88:889–897.
46. Polousky JD. Juvenile osteochondritis dissecans. *Sports Med Arthrosc.* 2011;19:56–63.
47. Saris DB, Vanlauwe J, Victor J, Haspl M, Bohnsack M, Fortems Y, Vandekerckhove B, Almqvist KF, Claes T, Handelberg F, Lagae K, van der Bauwhede J, Vandenneucker H, Yang KG, Jelic M, Verdonk R, Veulemans N, Bellemans J, Luyten FP. Characterized chondrocyte implantation results in better structural repair when treating symptomatic cartilage defects of the knee in a randomized controlled trial versus microfracture. *Am J Sports Med.* 2008;36:235–246.
48. Schagemann JC, Erggelet C, Chung HW, Lahm A, Kurz H, Mrosek EH. Cell-laden and cell-free biopolymer hydrogel for the treatment of osteochondral defects in a sheep model. *Tissue Eng Part A.* 2009;15:75-82.
49. Shin H, Quinten Ruhé P, Mikos AG, Jansen JA. In vivo bone and soft tissue response to injectable, biodegradable oligo(poly(ethylene glycol) fumarate) hydrogels. *Biomaterials.* 2003;24:3201–3211.
50. Shin H, Temenoff JS, Mikos AG. In vitro cytotoxicity of unsaturated oligo[poly(ethylene glycol) fumarate] macromers and their cross-linked hydrogels. *Biomacromolecules.* 2003;4:552–560.
51. Steadman JR, Briggs KK, Rodrigo JJ, Kocher MS, Gill TJ, Rodkey WG. Outcomes of microfracture for traumatic chondral defects of the knee: average 11-year follow-up. *Arthroscopy.* 2003;19:477–484.
52. Steinhagen J, Bruns J, Deuretzbacher G, Ruether W, Fuerst M, Niggemeyer O. Treatment of osteochondritis dissecans of the femoral condyle with autologous bone grafts and matrix-supported autologous chondrocytes. *Int Orthop.* 2010;34:819–825.
53. Stenhamre H, Nannmark U, Lindahl A, Gatenholm P, Brittberg M. Influence of pore size on the redifferentiation potential of human articular chondrocytes in poly(urethane urea) scaffolds. *J Tissue Eng Regen Med.* 2011;5:578–588.
54. Temenoff JS, Athanasiou KA, LeBaron RG, Mikos AG. Effect of poly(ethylene glycol) molecular weight on tensile and swelling properties of oligo(poly(ethylene glycol) fumarate) hydrogels for cartilage tissue engineering. *J Biomed Mater Res*. 2002;59:429–437.
55. Temenoff JS, Park H, Jabbari E, Conway DE, Sheffield TL, Ambrose CG, Mikos AG. Thermally cross-linked oligo(poly-(ethylene glycol) fumarate) hydrogels support osteogenic differentiation of encapsulated marrow stromal cells in vitro. *Biomacromolecules.* 2004;5:5–10.
56. Temenoff JS, Park H, Jabbari E, Sheffield TL, LeBaron RG, Ambrose CG, Mikos AG. In vitro osteogenic differentiation of marrow stromal cells encapsulated in biodegradable hydrogels. *J Biomed Mater Res A.* 2004;70:235–244.
57. Temenoff JS, Steinbis ES, Mikos AG. Effect of drying history on swelling properties and cell attachment to oligo(poly(ethylene glycol) fumarate) hydrogels for guided tissue regeneration applications. *J Biomater Sci Polym Ed.* 2003;14:989–1004.
58. Timmer MD, Shin H, Horch RA, Ambrose CG, Mikos AG. In vitro cytotoxicity of injectable and biodegradable poly(propylene fumarate)-based networks: unreacted macromers, cross-linked networks, and degradation products. *Biomacromolecules.* 2003;4:1026–1033.
59. Trinh TQ, Harris JD, Flanigan DC. Surgical management of juvenile osteochondritis dissecans of the knee. *Knee Surg Sports Traumatol Arthrosc.* 2012 February 11 [Epub ahead of print].
60. Wakitani S, Goto T, Pineda SJ, Young RG, Mansour JM, Caplan AI, Goldberg VM. Mesenchymal cell-based repair of large, full-thickness defects of articular cartilage. *J Bone Joint Surg Am.* 1994;76:579–592.
61. Yang Q, Peng J, Lu SB, Guo QY, Zhao B, Zhang L, Wang AY, Xu WJ, Xia Q, Ma XL, Hu YC, Xu BS. Evaluation of an extracellular matrix-derived acellular biphasic scaffold/cell construct in the repair of a large articular high-load-bearing osteochondral defect in a canine model. *Chin Med J (Engl).* 2011;124:3930–3938.
62. Yen YM, Steadman JR. Microfracture for osteochondritis dissecans lesions. *Oper Tech Sports Med.* 2008;16:77–80.
63. Yokota M, Yasuda K, Kitamura N, Arakaki K, Onodera S, Kurokawa T, Gong JP. Spontaneous hyaline cartilage regeneration can be induced in an osteochondral defect created in the femoral condyle using a novel double-network hydrogel. *BMC Musculoskelet Disord.* 2011;12:49.
64. Yoshizumi Y, Sugita T, Kawamata T, Ohnuma M, Maeda S. Cylindrical osteochondral graft for osteochondritis dissecans of the knee: a report of three cases. *Am J Sports Med*. 2002;30: 441–445.